Chapter-5

Pyrolysis of mustard straw: Evaluation of optimum process parameters, kinetic and thermodynamic study

5.1 Introduction

India is primarily an agricultural economy and has made spectacular progress in becoming more or less grain surplus. Besides producing cereals as a staple food, India also produces several oil-bearing fruits and seed-producing crops such as coconut, peanut, sesame seeds, rapeseeds (or mustard seeds), sunflower, etc. to meet its edible oil needs. Rapeseed or mustard seed (*Brassica spp.*) is the second most important oilseed produced in India after groundnut and meets around 27.8% of the vegetable oil needs of the country. The major rapeseed-growing Indian states are Gujarat, Haryana, Madhya Pradesh, Rajasthan, Uttar Pradesh, and some south Indian states. The plant takes around 105-160 days to mature, and the seeds have an average oil yield of 38 – 42% [135]. During 2017 – 2018, rapeseed cultivation covered an area of 5.96 million hectares with a total output of 8.32 million tons (i.e., around 1397 kg/hectare), respectively [136]. The solid material (also called meal) left after the oil extraction from the seed is used as animal feed. The stalk and pod husk account for about 70% of the whole mustard plant [137]. The people generally burn these for their household cooking purposes. This agricultural waste contains about 50% of the total plant energy and can be used as an energy source [138].

The present work was carried out with the aim of investigating the thermochemical characteristics and thermal degradation behavior of mustard straw. The measured residual weight-temperature data at different heating rates were used to evaluate the kinetic and thermodynamic parameters of the pyrolysis process with the help of isoconversional methods. The underlying reaction mechanism was elucidated using the Coats and Redfern 1964 method. In addition, the RSM technique with CCD was used to optimize the important operating variables like heating rate, gas flow rate, and temperature for obtaining the maximum amount of bio-oil. The product bio-oil was characterized using Fourier Transform Infra-red (FTIR) spectroscopy and Gas Chromatography-Mass Spectrometry (GCMS) techniques.

5.2 Physicochemical characterization of MS biomass

The physicochemical characterization of biomass was carried out by using proximate and ultimate analysis as per ASTM protocol (ASTM E871, ASTM E1755, and ASTM E872); however, C, H, N, and S (elemental analysis) were determined using an elemental analyzer (Euro, EA 3000 Italy). In addition, the calorific value of the biomass was computed by an oxygen bomb calorimeter (Rajdhani Scientific Instrument Company, New Delhi, India). Finally, the fiber analysis of biomass (cellulose, hemicellulose, and lignin) was estimated as per the method defined in section 3.2.7. The different functional groups in the MS biomass were identified using Fourier Transform Infrared Spectroscopy (FTIR, Model: FTS 3500 GX). The dried KBr powder was evenly mixed with the sample at a ratio of 1:100 and inserted into the sample container. Scanning was performed at 40 with a step size of 4 cm^{-1} within a 400 – 4000 cm^{-1} wavelength range.

5.3 Thermogravimetric analysis

The thermo-gravimetric analysis of MS powder was carried out using a Shimadzu TGA unit (TGA-50, Shimadzu Corporation, Tokyo, Japan) at the heating rates of 10, 15, 25, and 40 °C/min under an inert nitrogen environment (100 ml/min) upto the temperature of 800°C.

5.4 Kinetic analysis

There are basically three different techniques used for calculating kinetic parameters. The first method is based on the multiple linear regression (MLR) technique, in which TGA data collected at a single heating rate was analyzed. The second approach is established on the implementation of model-free methods, which need at least three distinct heating rates. The third methodology was given by Coats and Redfern (1964), which includes fitting of reaction-based model utilizing TGA data at a single heating rate [77]. This study used isoconversional models (KAS, OFW, and VZK) and reaction fitting-based models (Coats-Redfern) to analyse the TGA data. The equation and assumption related to these models are available in earlier

section 3.5, whereas values of g(α) for different solid-state reaction mechanisms are presented in Table 3.1.

5.5 Pyrolysis Experimental setup

The batch pyrolysis of MS feedstock was investigated in a laboratory-scale fixed bed reactor (SS, height: 42 cm, inner diameter: 4.5 cm) (Fig. 3.2). The pyrolysis setup had an externally heated PID-controlled furnace to supply the energy required for pyrolysis. The reactor had two openings, one at the top for introducing N_2 gas and the second at the bottom for removing volatiles (condensable and non-condensable gases). A water-cooled glass condenser and a collecting vessel immersed in an ice bath were connected to the bottom of the reactor for complete condensation of the condensable volatiles. About 25 g of accurately weighed biomass was taken into the reactor, and N_2 gas was purged for 20 minutes prior to the experiment in order to create an inert atmosphere. As the temperature reached the set value, the condensable volatiles was collected in the ice-cooled vessel while the non-condensable portions were vented off, whereas the solid portion (char) was left in the reactor. The yield of the products was determined using the below-mentioned equation.

$$\text{Bio-oil yield (wt.\%)} = \frac{\text{Bio-oil weight}}{\text{Biomass weight}} \text{x}100 \quad (5.1)$$

$$\text{Biochar yield (wt.\%)} = \frac{\text{Biochar weight}}{\text{Biomass weight}} \text{x}100 \quad (5.2)$$

$$\text{Gases yield (wt.\%)} = 100 - (\text{bio-oil yield} + \text{biochar yield}) \quad (5.3)$$

5.6 Design of Experiments (DOE)

The design expert software (Version 11, Stat-Ease USA) was used for the optimization of pyrolysis process parameters. Temperature (coded as A), heating rate (coded as B), and sweeping gas flow rate (coded as C) were selected as independent variables, while the dependent variable was bio-oil yield. The design was composed of six axial points, eight

factorial points, as well as six centre points, replicates at 5 different levels (-1, +1, 0, -alpha, +alpha), comprising of a series of 20 experiments as assessed from Eq. (5.4) shown below [77].

$$N = 2^n + 2n + n_c = 2^3 + 2 \times 3 + 6 = 20 \quad (5.4)$$

where N indicates required overall mandatory trials, and n denotes the number of factors. The result of all the experiments was fitted into a second-degree model (Eq. 5) [77].

$$Y = \beta_o + \sum_{i=1}^{n} \beta_i X_i + \sum_{i=1}^{n} \beta_{ii} X_i^2 + \sum_{i=1}^{n} \sum_{j>1}^{n} \beta_{ij} X_i X_j \quad (5.5)$$

where Y is the predicted response, n is the total number of experiments, β_o, β_i, β_{ii}, β_{ij} are the regression coefficients for the constant, linear, quadratic, and interaction terms; however, independent factors were coded as X_i *and* X_j. On the basis of three factors (temperature, heating rate, and sweeping gas flow rate), an optimized yield of the bio-oil was analyzed with the help of ANOVA ("analysis of variance") for the final model.

5.7 Bio-oil characterization

The viscosity of the bio-oil was measured by employing a Brookfield viscometer, whereas higher heating value (HHV) was measured by employing a bomb calorimeter (RD Scientific, New Delhi). The pH of the bio-oil was evaluated using a pH meter (Toshcon, Ajmer, India) and its density was calculated using a graduated flask and electronic weighing balance. Air oven and muffle furnace were used to measure the ash content of the bio-oil. FTIR spectroscopy (Model: Nicolet iS5) was employed to recognize functional groups in the bio-oil. Further, GCMS analysis (Shimadzu QP-2010 plus) equipped with a column (Rxi-5 MS) having dimensions (30 m x 0.25 mm ID and 0.25 μm film thickness) was employed to identify the unknown organic compounds. GC oven was initially held at 50°C for 4 minutes, then the temperature was increased to 280°C at 4 °C/min and held there for 30 minutes. The injector and detector temperature was set at 250°C and 280°C, respectively. Helium gas (with flow rate

= 1 ml/min) was utilized as the carrier gas. The compounds in the bio-oil were recognized by matching the mass spectra with the NIST library database.

5.8 Results and discussion

5.8.1 Characteristics

The physicochemical characteristics (Table 5.1) of MS biomass have been compared with those of some other reported biomasses like cotton stalk, rice straw, and wheat straw [140]. It was found that the MS biomass has a lower ash content (5.02%) and higher volatile matter (75.55%). Biomass having lower ash content and higher volatile matter tend to have higher ignition efficiency; in contrast, higher ash level act as a heat sink and increases the chance of slagging as well as fouling within the furnace and boiler [100]. The low moisture content (3.99%) compared to the threshold limit of 10% indicates its high suitability for pyrolysis. However, this is not the alone criteria in deciding the biomass for pyrolysis [100]. The moderate content of fixed carbon (15.44%) indicates its suitability as bio-adsorbents, solid fuels, bio-fertilizer, and soil amendment [100,141]. Further ultimate analysis (CHNS) confirmed carbon, hydrogen, and nitrogen to be 54.46%, 6.29%, and 0.5%, respectively, with no sulfur content. The presence of lower nitrogen and negligible sulfur has the advantage in emission of lower NO_x and SO_x during the pyrolysis process [100]. In addition, HHV of MS feedstock was obtained to be 16.88 MJ/kg, whereas bulk density was obtained to be 397.2 kg/m^3. Fiber analysis of MS biomass revealed hemicellulose (23.12%), cellulose (44.5%), and lignin (21.24%). The obtained results in this study are consistent with other published data compared in this study.

Table 5.1: Physiochemical properties of MS biomass with comparison to other biomass

Analysis	MS biomass	Cotton stalk [140]	Rice straw [140]	Wheat straw [140]
Proximate analysis (wt. %)				
Moisture content[a]	3.99	8.9	10.0	10.6

Volatile matter[b]	75.55	71	65.0	63.0
Ash content[b]	5.02	3.5	13.7	10.5
Fixed Carbon[b,c]	15.44	16.6	11.3	15.9
Ultimate analysis (%)				
Carbon[b]	54.46	46.8	38.8	41.7
Hydrogen[b]	6.29	6.4	6.7	5
Oxygen[b]	38.75	46.8	38.8	41.7
Nitrogen[b]	0.5	0.3	0.2	0.4
Sulfur[b]	–	0.2	0.2	0.3
O/C ratio	0.53	0.75	0.75	0.75
H/C ratio	1.38	1.64	2.07	1.43
Fiber analysis (wt. %)				
Hemi-cellulose[b]	23.12	19.2	19.9	18.9
Cellulose[b]	44.5	39.4	38.1	36.6
Lignin[b]	21.24	23.2	11.9	20.3
Heating value (MJ/kg)	16.88	19.2	16.2	17.4
Bulk density[a] (kg/m^3)	397.2	–	–	–

[a] Wet basis; [b] Dry basis; [c] By difference

5.8.2 Thermal study

Thermal investigation of MS feedstock was accomplished in a thermogravimetric analyzer at 10 °C/min in the temperature range of 23 to 800°C. The thermal analysis of MS biomass depicts the typical behavior of pyrolysis of lignocellulosic biomass as presented in Fig. 5.1 (a). It is seen that there exists three main degradation zone (drying, devolatilization, and char formation zone) [88]. The drying region (23 – 162°C) attributes to the release of H_2O and few light-weight (volatile) molecules retained in MS biomass. The active pyrolysis region (162 – 500°C) is the major devolatilization zone due to the deterioration of cellulose and hemicellulose in the feedstock. In this region, large molecular weight compounds are transformed into low molecular weight species that constitute combustible and non-combustible gases like CH_4, H_2,

CO, hydrocarbons, CO_2, and N_2 [142]. In the passive pyrolysis region (>500°C), the deterioration of lignin takes place at a slower rate confirming its higher thermal stability due to the presence of hydroxyl phenolic groups [63,143]. The DTG plot shown in Fig 5.1 (a) reveals that the first peak observed at around 52°C is due to the evaporation of water as well as some light volatile molecules. The second peak observed at around 284 and 322°C is associated with the degradation of cellulose & hemicellulose, respectively. At higher temperatures (>500°C), the decomposition peak is relatively insignificant because lignin degrades at a slower rate. The thermal analysis indicated 7.7, 63.2, and 14.22 wt. % loss of MS biomass in the 1^{st}, $2^{nd,}$ and 3^{rd} regions, respectively.

5.8.3 Impact of heating rates

The effect of hearing rate on TG-temperature and DTG-temperature profiles is shown in Fig. 5.1 (a) through 5.1 (d). It is seen from Fig. 5.1 that there is a gradual shift in the profile and peaks towards the higher temperature region. The peak observed at 234°C for 10°C/min heating rate has shifted to 246, 248, and 266°C for 15, 25, and 40°C/min heating rates, respectively. This shift can be attributed to the low rates of intra-particle heat transfer and the formation of heavier molecules and tar through secondary reactions [7,144]. Pyrolysis of biomass at lower heating rates is more appropriate to accomplish complete biomass transformation due to increased heat transfer; however, it may affect the projected product constituents by creating a secondary pyrolysis reaction. In addition, at a higher heating rate, biomass particles dispersed rapidly and formed hot volatiles, which escaped rapidly from the reactor (lessen residence time). This causes the formation of the product of the anticipated constituent and clarifies the inference that fast pyrolysis is better than slow pyrolysis [26]. Further, it was seen from Fig. 5.1 that with an upsurge in heating rate thermal breakdown of cellulose, hemicellulose and lignin changed [7,101]. The hemicellulose decomposition peak shifted to 284 to 287°C, 294, and 317°C, while the cellulose decomposition peak shifted to 322 to 325°C, 343, and 354°C.

Ashraf et al., (2019) have reported that degradation of cellulose, hemicellulose, and lignin takes place in the temperature range of 150 – 360, 240 – 400°C, and greater than 500°C, respectively, and these temperature ranges also depend upon the nature of biomass. It is important to note that the percentage residual weight increases in the order of 16.30, 16.94, 19.14, and 19.38%, with an increase in the heating rate from 10, 15, 25 to 40°C/min, respectively. The ash content gets diminished at a lower heating rate, and it gets enhanced at a higher heating rate due to incomplete pyrolysis at a higher heating rate [7].

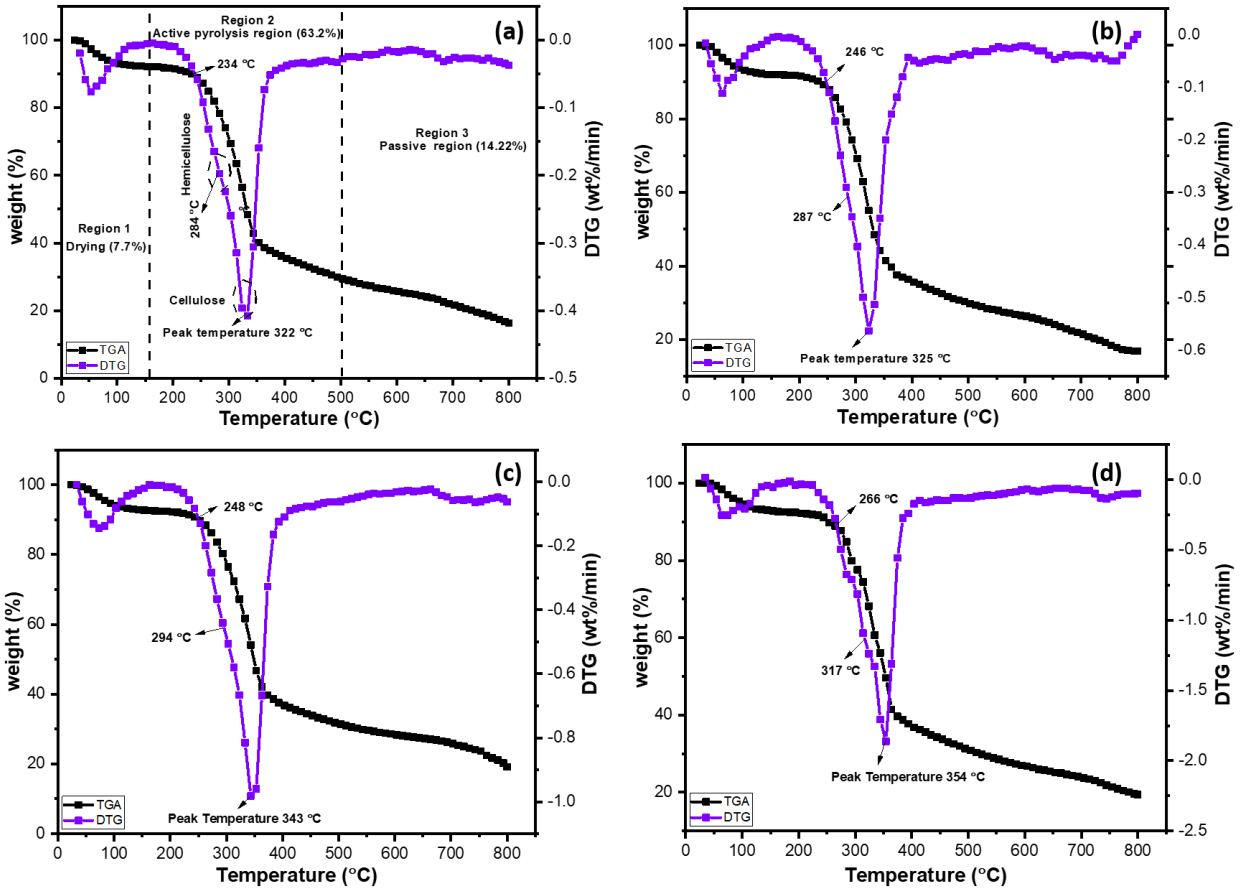

Fig. 5.1: TG and DTG curves of MS biomass at a heating rate of a) 10, b) 15, c) 25, and d) 40 °C/min

5.8.4 Kinetic analysis using isoconversional methods

The activation energy of the thermal degradation of MS biomass was calculated from the slopes of the linear plot of KAS, OFW (Fig. 5.2), and Vyazovkin models as approved by the ICTAC kinetics committee and are presented in Table 5.2. The correlation coefficient (R^2) was greater

than 0.92 for each model at all fractional conversions confirming their suitability for analyzing the experimental data [147]. The activation energy values varied from 222.89 – 152.56 kJ/mol, 225.46 – 144.48 kJ/mol, and 225.64 – 145.21 kJ/mol, whereas average activation energy values were 202.19, 201.80, and 202.12 kJ/mol employing KAS, OFW, and Vyazovkin method respectively. The observed variation in activation energy values with increasing conversion is due to the variation in the nature and reactivity of the degradation products formed out of cellulose, hemicellulose, and lignin [97]. It was clear from Table 5.2 that the change of activation energy with conversion indicates biomass breakdown followed multistep reactions [147]. It was reported that activation energy depends on pyrolysis reaction and can be used in the fuel reactivity calculation, which means if the activation energy value is high, then pyrolysis reaction is slower or vice-versa [148]. Fuel reactivity has a major impact on biomass pyrolysis and gasification. It plays an important role in the sketching, design, and creation of a new pyrolysis setup [63].

The effect of activation energy with progressive conversion is shown in Fig. 5.3. It can be observed from Fig. 5.3 that there is a slight variation in activation energy value among the different types of models used in this study. This slight variation in activation energy was owing to the variation in approximation used by the respective models. However, it is important to remember that every biomass has a particular range of temperature for deterioration which is influenced by the biomass composition. The activation energy depends on biomass types, mathematical equations, and operating conditions for pyrolysis. As per the "International Confederation for Thermal analysis and Calorimetry" (ICTAC), Vyazovkin model gives a better evaluation of apparent activation energy value, whereas KAS has a higher error than OFW [111].

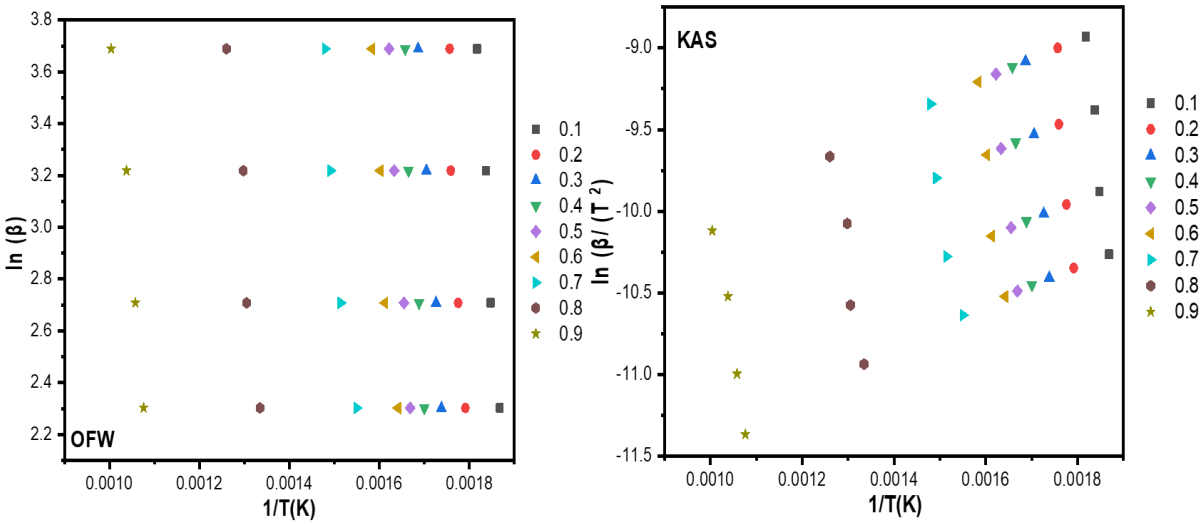

Fig. 5.2: Arrhenius plot for calculation of activation energy using OFW and KAS

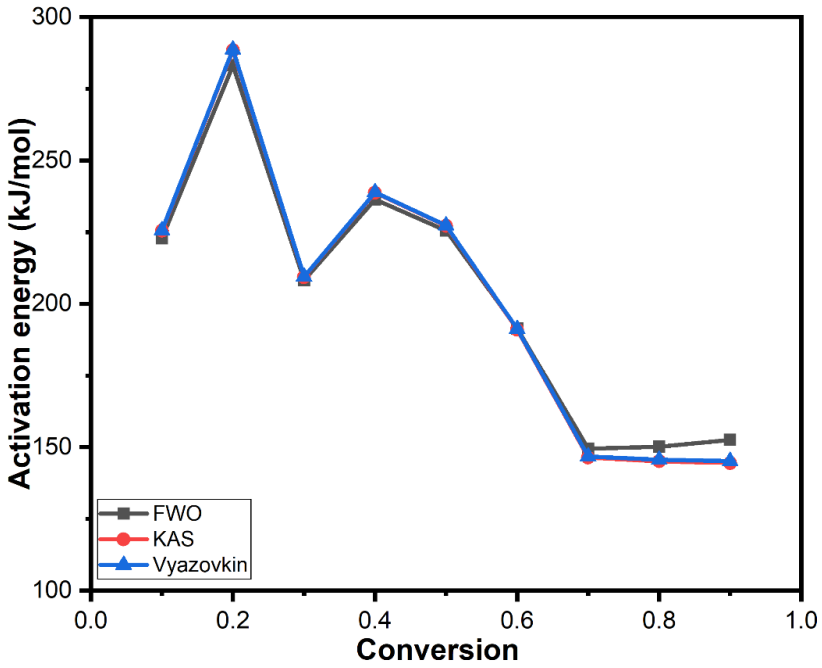

Fig. 5.3: Change in activation energy with respect to progressive conversion

Table 5.2: Kinetic analysis of MS biomass using model free methods

Conversion	OFW	R^2		KAS	R^2		VZK
	Equation		E(kJ/mol)	Equation		E(kJ/mol)	E(kJ/mol)
0.1	y = -28203x + 54.948	0.974	222.89	y = -27118x + 40.355	0.972	225.46	225.64
0.2	y = -35824x + 66.416	0.921	283.11	y = -34697x + 51.746	0.916	288.47	288.71
0.3	y = -26346x + 48.137	0.995	208.21	y = -25178x + 33.397	0.995	209.33	209.53
0.4	y = -29912x + 53.17	0.969	236.39	y = -28720x + 38.39	0.967	238.77	238.95
0.5	y = -28544x + 49.929	0.988	225.58	y = -27329x + 35.109	0.987	227.21	227.41
0.6	y = -24215x + 41.963	0.945	191.37	y = -22976x + 27.104	0.939	191.02	191.28
0.7	y = -18921x + 31.534	0.936	149.53	y = -17601x + 16.549	0.927	146.38	146.74
0.8	y = -18997x + 27.666	0.932	150.13	y = -17454x + 12.369	0.921	145.11	145.61
0.9	y = -19304x + 23.132	0.978	152.56	y = -17378x + 7.3918	0.973	144.48	145.21
	Average		202.19	Average		201.80	202.12

5.8.5 Model fitting kinetics

The activation energy corresponding to the most commonly applied solid-state procedures *g(α)* are listed in Table 5.3 at heating rates of 10, 15, 25, as well as 40 °C/min. The activation energies obtained using OFW, KAS, and Vyazovkin were chosen because they are independent of a particular kinetics mechanism. The activation energy from the CR approach was utilized to estimate the governing reaction mechanism. The most suitable reaction mechanism was determined using the measured activation energy values of the CR approach by comparing it with model-free methods. As seen in Table 5.3, activation energy values obtained using the CR method were too small; hence a higher-order model was employed to determine the governing reaction mechanism. Lara et al., (2017) suggested that the fourth and fifth-order models must be accountable for the pyrolysis of olive tree pruning. F_n model ($f_x = (1-x)^n$) (n is in between 3 and 4) was suggested by Aslan et al., (2017) for pyrolysis of waste tires. Hence, in the current study, activation energy values obtained from the F5 model for heating rates of 10°C/minute is 145.28 kJ/mol, for 15°C/min is 138.51 kJ/mol, for 25°C/min is 158.27 kJ/mol, and for 40°C/min is 153.75 kJ/mol which is close to KAS, OFW, and Vyazovkin method as seen from Table 5.2 and Table 5.3. Therefore, random nucleation (5^{th} order) with five nuclei on the individual particle is the most suitable reaction mechanism for the thermal degradation of MS biomass.

Table 5.3: Kinetic analysis of MS biomass using CR method

Reaction model	10 °C/min	R^2	15 °C/min	R^2	25 °C/min	R^2	40 °C/min	R^2
	E_α		E_α		E_α		E_α	
A1	34.91	0.949	29.74	0.861	34.20	0.951	33.73	0.924
A2	23.74	0.937	19.83	0.828	23.15	0.939	22.77	0.906
A3	12.58	0.900	9.91	0.724	12.09	0.900	11.81	0.849
A4	7.00	0.827	4.96	0.529	6.56	0.818	6.33	0.733
R1	42.96	0.913	37.73	0.827	40.66	0.901	40.40	0.870

R2	49.67	0.938	43.35	0.859	47.92	0.935	47.50	0.908
R3	52.09	0.945	45.36	0.869	50.59	0.944	50.10	0.919
F1	57.24	0.957	49.58	0.886	56.31	0.960	55.65	0.938
F2	74.97	0.979	63.95	0.926	76.53	0.984	75.16	0.972
F3	95.95	0.985	80.71	0.950	100.90	0.986	98.57	0.983
F4	119.59	0.982	105.12	0.946	128.46	0.978	125.06	0.982
F5	145.28	0.976	138.51	0.941	158.27	0.968	153.75	0.977
D1	95.66	0.930	85.38	0.861	91.34	0.921	90.92	0.897
D2	104.09	0.943	92.49	0.877	100.36	0.938	99.76	0.915
D3	113.93	0.955	100.63	0.892	111.19	0.955	110.31	0.933
D4	107.35	0.947	95.19	0.882	103.94	0.944	103.25	0.922

5.8.6 Thermodynamic analysis

The thermodynamic study was conducted at each heating rate (10, 15, 25, and 40°C/min) to see the impact of heating rate on thermodynamic parameters using activation energy achieved from the Vyazovkin method that was presented in Table 5.4. The average value of "pre-exponential factor" (A) was computed to be 1.12513E+24, 8.45895E+23, 1.51309E+23 and 5.70831E+22, whereas it altered from 1.29395E+12 to 1.01258E+25, 1.12512E+12 to 7.61272E+24, 4.67566E+11 to 1.3617E+24 and 2.88313E+11 to 5.13712E+23 at heating rates of 10, 15, 25 and 40°C/min respectively. This high alteration in frequency factor corresponds to the complex reaction mechanism exhibited by MS biomass during pyrolysis [106]. The average value of change in enthalpy (ΔH) was observed to be 196.77, 196.70, 196.63, as well as 196.55 kJ/mol, whereas it varied from 137.48 to 284.07 kJ/mol, 137.35 to 284.03 kJ/mol, 137.2 to 283.98 kJ/mol and 136.93 to 283.98 kJ/mol corresponding to heating rates of 10, 15, 25 and 40°C/min. The difference between activation energy and enthalpy change was found to be (~5). This little difference suggests that the pyrolysis of MS biomass easily overcame the potential energy barrier and product formation is viable [151]. Gibb's free energy (ΔG)

represents the energy stored in the reactants during pyrolysis. Higher the value of ΔG, higher the energy required by the system during pyrolysis, whereas lower ΔG suggests the product can also be produced well with less energy requirement. The average ΔG value was observed to be 154.89, 155.66, 160.63 as well as 163.52 kJ/mol, whereas it altered from 152.99 to 156.39 kJ/mol, 153.75 to 157.17 kJ/mol, 158.66 to 162.18 kJ/mol and 161.51 to 165.1 kJ/mol with respect to heating rates of 10, 15, 25 and 40°C/min. The obtained value suggests that MS biomass has enough capability to be transformed into energy through the pyrolysis process. Change in entropy (ΔS) is the degree of randomness in the system. The value of ΔS is positive up to conversion from 0.1 to 0.6, whereas it gets negative from 0.7 to 0.9. The negative value denotes that thermal equilibrium has been achieved, and the product formed is thermally stable [152]. Further, heating rate has very little effect on the thermodynamic parameters (Table 5.4). The pre-exponential factor decreases with an increase in heating rate, whereas enthalpy has a negligible effect. Gibb's free energy change has been increased, whereas the change in entropy value decreases at a particular conversion with an increase in heating rate.

Table 5.4: Thermodynamic analysis of MS biomass at heating rate of 10, 15, 25 and 40 °C/min

Conversion	$A(s^{-1})$	ΔH(kJ/mol)	ΔG(kJ/mol)	ΔS(J/mol)	$A(s^{-1})$	ΔH(kJ/mol)	ΔG(kJ/mol)	ΔS(J/mol. K)
	10°C/min				**15°C/min**			
0.1	2.30519E+19	221.19	154.21	112.54	1.84749E+19	221.14	154.98	110.61
0.2	1.01258E+25	284.07	152.99	220.24	7.61272E+24	284.03	153.75	217.8
0.3	8.25193E+17	204.75	154.58	84.293	6.72239E+17	204.71	155.35	82.53
0.4	3.59601E+20	234.06	153.93	134.64	2.8434E+20	234.03	154.69	132.63
0.5	3.32241E+19	222.43	154.17	114.68	2.65797E+19	222.39	154.94	112.76
0.6	1.88439E+16	186.22	155.03	52.39	1.56377E+16	186.12	155.8	50.69
0.7	1.78138E+12	141.38	156.34	-25.14	1.54656E+12	141.25	157.12	-26.53
0.8	1.40676E+12	139.38	156.38	-28.56	1.22272E+12	139.24	157.16	-29.95
0.9	1.29395E+12	137.48	156.39	-31.77	1.12512E+12	137.35	157.17	-33.13
Average	1.12513E+24	196.77	154.89	70.36	8.45895E+23	196.7	155.66	68.6
	25°C/min				**40°C/min**			
0.1	4.78664E+18	221.12	159.92	99.31	2.24106E+18	221.07	162.8	92.91
0.2	1.3617E+24	283.98	158.66	203.4	5.13712E+23	283.98	161.51	195.3
0.3	1.91457E+17	204.65	160.3	71.98	9.47218E+16	204.6	163.19	66.04

0.4	6.81285E+19	233.96	159.63	120.6	3.04761E+19	233.93	162.5	113.9
0.5	6.81526E+18	222.32	159.88	101.3	3.17156E+18	222.28	162.76	94.92
0.6	4.9577E+15	186.09	160.77	41.1	2.61093E+15	186.03	163.66	35.67
0.7	6.36952E+11	141.17	162.13	-34.02	3.90709E+11	141.12	165.04	-38.1
0.8	5.06931E+11	139.21	162.17	-37.27	3.12159E+11	139.01	165.08	-41.6
0.9	4.67566E+11	137.2	162.18	-40.54	2.88313E+11	136.93	165.1	-44.9
Average	1.51309E+23	196.63	160.63	58.44	5.70831E+22	196.55	163.52	52.67

5.8.7 Optimization of process parameters

RSM was used to analyze the concurrent impact between process response and independent variables based on the central composite design (CCD) technique. A total of 20 experimental runs were performed, consisting of six axial, six central, and eight factorial points. Table 5.5 describes the CCD experimental design matrix and outcomes using three variables. The process response (bio-oil yield) and independent variables (temperature, heating rate, and N_2 gas flow rate) were expressed in the form of coded factors as given below:

$$Biooil\ yield\ (wt\ \%) = +44.33 + 1.43A + 0.3723B + 0.0721C - 2.05A^2 - 1.90B^2 - 0.3164C^2 + 0.3662AB + 0.1237BC - 0.2163BC$$

where A, B, and C are independent variables, namely temperature (°C), heating rate (°C/minute), and N_2 gas flow rate (ml/minute). The experimental and predicted value of bio-oil yield (wt %) ranged from 38.37 – 44.69% and 38.38 – 44.33%, respectively, whereas the optimized condition for bio-oil yield was (temperature = 500°C, heating rate = 25 °C/minute, and sweeping gas flow rate = 100 ml/minute). To analyze the value of each variable and assess the model accuracy, ANOVA was used for pyrolysis of MS biomass, and the results are presented in Table 5.6. The terms F (Fisher's test) and 'p' were evaluated to understand the significance of the model. Higher F-value and lower p-value indicate the model to be significant. In this study, a high F-value (208.54) and lower p-value (<0.0001) indicate that the model is significant. From Table 5.6, linear (A and B), quadratic (A^2 and B^2), and interaction terms (AB and BC) have p-values lower than 0.0500, which indicate that the terms are noteworthy. However, the individual term (C), its quadratic term (C^2), and the interaction term (AC) were non-significant due to p-values higher than 0.0500 (Table 5.6). The F-value for temperature (317.72) was higher in comparison to that for the heating rate (23.55) and gas flow rate (0.9420) which indicate that the temperature has a substantial impact on the bio-oil formation compared to heating rate and N_2 gas flow rate. A similar observations have been

reported by Mishra et al. (2020c), Brown and Brown (2012), and Kiliç et al. (2014). Furthermore, interconnecting terms such as temperature-heating rate (AB), heating rate-gas flow rate (BC), and gas flow rate-temperature (CA) did not have much effect on pyrolytic liquid formation due to the small F-value. F-value for quadratic term A^2 (temperature) was much higher (498.63) than "heating rate" (B^2) and N_2 flow rate (C^2), summarizing that "temperature" (A^2) has a greater impact on bio-oil yield. These results indicated that the N_2 gas flow rate had not altered the bio-oil formation significantly. The correlation between experimental and expected values is portrayed in Fig. 5.4, showing that the expected and experimental results are very similar, and the coefficient of correlation (R^2=0.9947) is near 1, suggesting the model fitted closely with the actual data.

3D plots are used to categorize and correlate the interconnection between different process parameters and response yield. Fig. 5.5 (a) through 5.5 (c) illustrated the three-dimensional and contour plots of response variables with respect to bio-oil yield. As seen from Fig. 5.5, it can be said that temperature significantly affects pyrolytic liquid yield more than the heating rate. It has been concluded from the present outcome that the maximum bio-oil yield of 44.69% was attained at a temperature of 500°C, a sweeping gas flow rate of 100 ml/minute, and a heating rate of 25 °C/minute.

Table 5.5: Central composite design (CCD) matrix and results

Run	Factor 1 A:Temperature (°C)	Factor 2 B:Heating rate (°C /min)	Factor 3 C:sweeping gas flow rate (ml/min)	Response	
				Predicted bio-oil yield (%)	Actual bio-oil yield (%)
1	500	25	100	44.33	44.43
2	400	10	50	38.47	38.56
3	500	25	60	44.07	44.13
4	600	40	150	42.21	42.08
5	500	25	150	44.08	44.18

6	600	40	50	42.25	42.27
7	500	25	100	44.33	44.25
8	400	40	50	38.91	38.78
9	668.179	25	100	40.93	41.02
10	500	40	100	42.80	43.01
11	400	10	150	38.80	38.74
12	600	10	150	41.16	41.26
13	550	25	100	44.53	44.1
14	500	25	100	44.33	44.31
15	500	17	100	43.59	43.33
16	400	40	150	38.38	38.37
17	600	10	500	40.34	40.31
18	500	25	100	44.33	44.38
19	500	25	100	44.33	44.69
20	500	25	100	44.33	44.27

Table 5.6: Results of ANOVA for the response of MS bio-oil using a quadratic model

Source	Sum of squares	Df	Mean square	F-value	p-value	Remark
Model	98.68	9	10.96	208.54	<0.0001	Significant
A-Temperature	16.70	1	16.70	317.72	<0.0001	
B-Heating rate	1.24	1	1.24	23.55	0.0007	
C-Sweeping gas flow	0.0495	1	0.0495	0.9420	0.3546	
AB	1.07	1	1.07	20.41	0.0011	
AC	0.1225	1	0.1225	2.33	0.1579	
BC	0.3741	1	0.3741	7.12	0.0236	
A^2	26.22	1	26.22	498.63	<0.0001	
B^2	6.97	1	6.97	132.66	<0.0001	
C^2	0.2018	1	0.2018	3.84	0.0785	
Residual	0.5258	10	0.0526			
Lack of Fit	0.3937	5	0.0787	2.98	0.1279	Not significant

Pure Error	0.1321	5	0.0264			
R^2	0.9947					
Cor. Total	99.20	19				

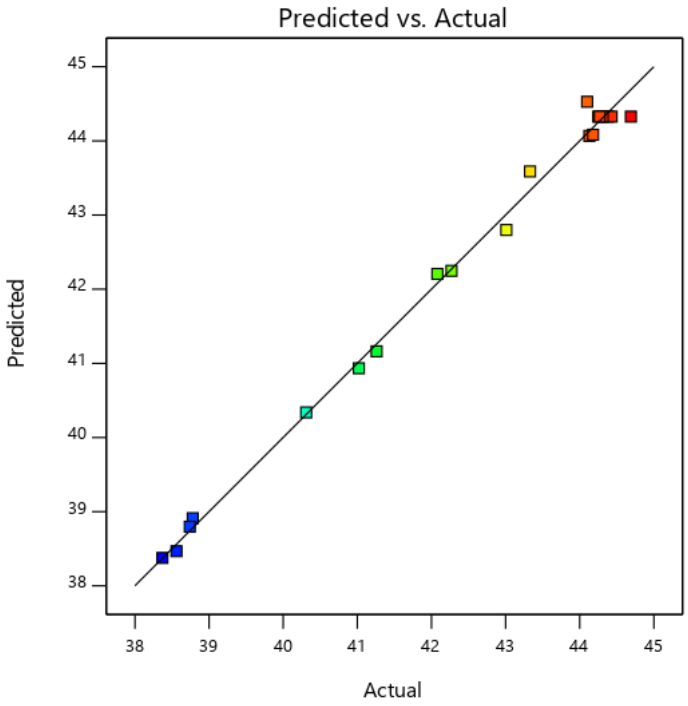

Fig. 5.4: Comparison of experimental and predicted bio-oil yield

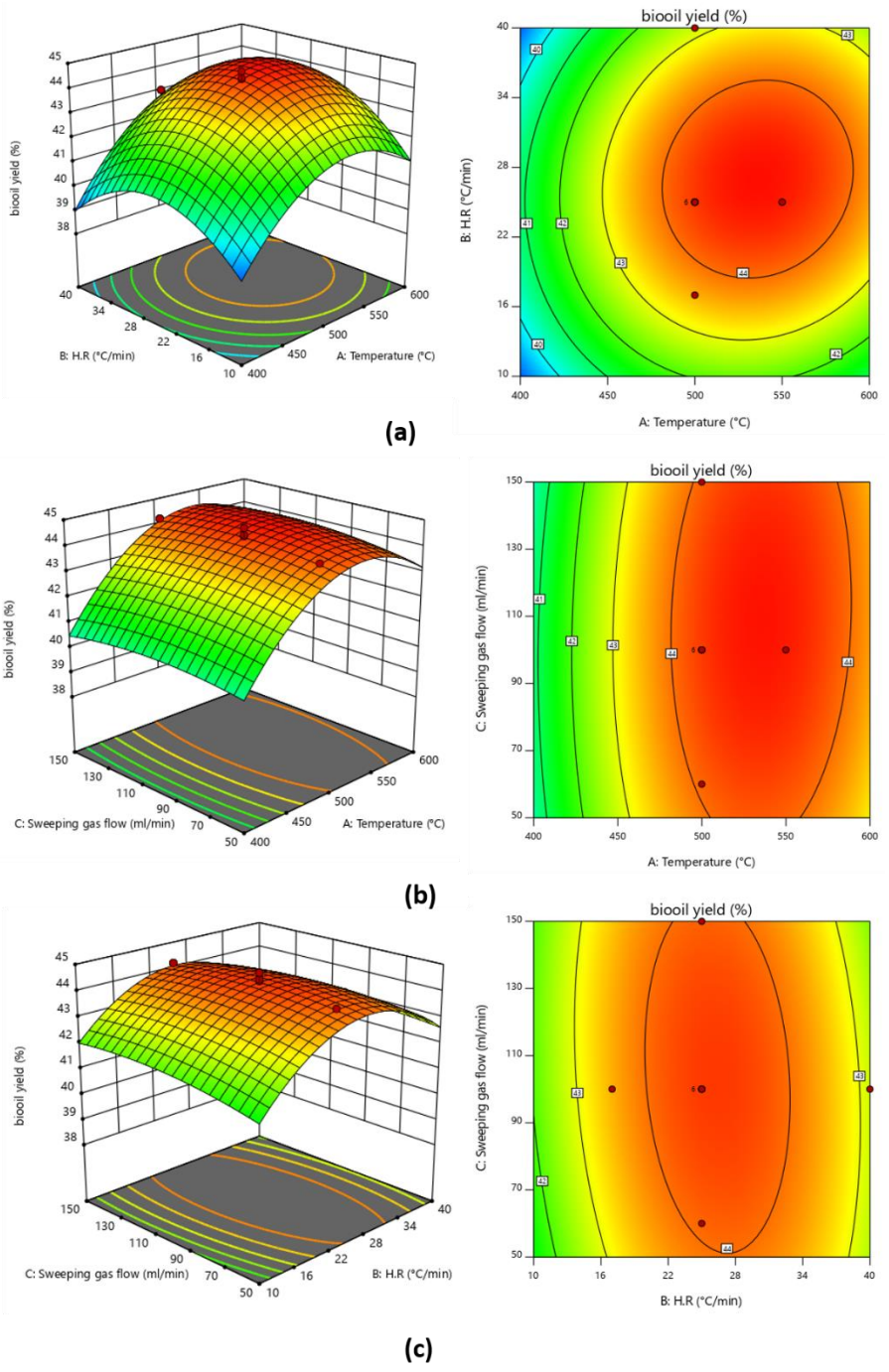

Fig. 5.5: Three-dimensional response surface and bio-oil yield contour plots against (a) heating rate and temperature (b) sweeping gas flow rate and temperature (c) heating rate and sweeping gas flow rate

5.8.8 Bio-oil characterization

Pyrolytic liquid procured under optimum pyrolysis conditions (temperature = 500°C, sweeping gas flow rate = 100 ml/minute, and heating rate = 25°C/minute) has been characterized and compared with commercial diesel fuel as shown in Table 5.7. The bio-oil has a lower pH value

(2.49) which negatively impacted the higher heating value. The low pH value is due to higher organic acids, which necessitate further up-gradation of bio-oil to prevent corrosion and its use as a liquid fuel [69]. The viscosity of the bio-oil is found to be 4.64 cSt at 30°C, 50 rpm, and is comparable to diesel fuel. Higher viscosity directly influences stability, fluidity, and flame temperature [61,119,153]. Viscosity also plays a significant role in the design and injection of fuel [154]. The high density of bio-oil (1032 kg/m^3) might be due to the formation of different types of complex molecules as well as metal-bearing compounds [62]. The low HHV value of the bio-oil (20.31 MJ/kg) than the diesel fuel is due to the higher concentration of organic acids in the bio-oil. Bio-oil ash content was observed to be 0.21%. Finally, Ramsbottom carbon residue of the bio-oil was found to be 2.11%, which corresponds to the carbon forming tendency of the bio-oil at elevated temperatures.

Table 5.7: Characteristics of MS bio-oil and diesel

Analysis	MS bio-oil	Diesel
Color	Brown	–
Odour	Smoky	–
pH	2.49	–
Density(kg/m^3)	1032	820
Viscosity (cSt) (30 °C) (50 rpm)	4.64	2–4.5
Ash Content (wt. %)	0.21	–
HHV (MJ/kg)	20.31	45.5
Ramsbottom carbon residue (wt. %)	2.11	–

5.8.9 FTIR analysis of MS biomass and bio-oil

The functional group present in the MS biomass and the bio-oil were identified through FTIR spectroscopy as shown in Fig. 5.6. The absorption band present in the wave number range 3369 – 3403 cm^{-1} can be linked to the –OH group of alcohol, protein, phenol, water, and aromatic phenols [99]. The presence of a peak at 2924 cm^{-1} is due to C–H stretching of alkane and saturated aliphatic group, whereas the absorption band found in the range 2097 – 2146 cm^{-1} is attributed to –C≡N, group of aliphatic cyanide and nitriles [122]. The presence of the peak in

the range 1716 – 1735cm^{-1} is due to C=O stretching vibration. It confirms the existence of carboxylic acid and ester. In contrast, the peak at 1508 – 1643 cm^{-1} is due to the C=C aromatic ring and reveals the existence of protein and lignin [122,155]. The peak at 1422cm^{-1} is attributed to the -CH, -CH_2, and -CH_3 bending vibration in alkanes, whereas the peak corresponding to 1379 cm^{-1} is because of the stretching of –CH and aliphatic –CH, indicating the existence of methyl and phenol [123]. The peak at 1244-1268 cm^{-1} is due to –CH stretching vibrations indicating the presence of alkanes [123], and the peaks at 1054 cm^{-1} and 1050 cm^{-1} are due to C=O stretching vibrations of ethers and esters. The peaks at 612 cm^{-1} as well as 655 cm^{-1} are due to the existence of mono and polycyclic aromatic compounds in the bio-oil and biomass [144].

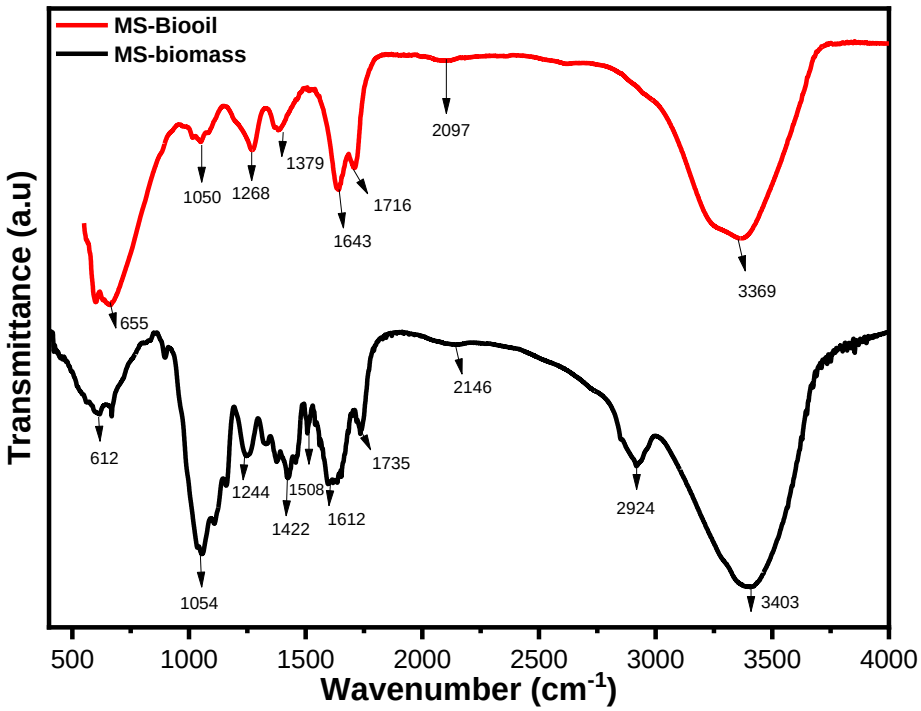

Fig. 5.6: FTIR analysis of MS biomass and MS bio-oil

5.8.10 GCMS analysis

The GCMS analysis of the product bio-oil at the optimized pyrolysis condition was performed to identify the types of chemical compounds present in the MS bio-oil with the help of the NIST library, as shown in Fig. 5.7. The detailed compound list is presented in Appendix E.

Bio-oil is a complex mixture of nitrogen-containing, oxygenated, benzene derivatives, aliphatic organic compounds in ample quantities. These compounds cause bio-oil more proficient for wide application in an engine [61]. The complex nature of the bio-oil is due to the complex nature of the biomass (cellulose, hemicellulose, and lignin). However, constituents of these compounds change with types of biomass, pyrolysis operating conditions, etc. It can be seen from the result (Fig. 5.7) that bio-oil contains: hydrocarbons (33.52%), acids (7.53%), ester (25.18%), ketone (10.91), alcohol (13.31%), amide (2.91%), aldehyde (0.27%), nitrile compounds (0.38%) and nitrogen-containing compounds (0.72%). The major constituents of bio-oil are: 4-tert-Butylcyclohexyl acetate (22.7%), docosane (16.30%), Bicyclo[7.2.0]undec-4-ene, 4,11,11-trimethyl-8-methylene-, [1R-(1R*,4E,9S*)] (13.56%), 2-Pentanol, 3-methylene (7.55%), Bicyclo[7.2.0]undec-4-ene, Acetyl valeryl (6.94%), Disulfide, dioctyl (4.98%), Oxalic acid, dineopentyl ester (4.24%), Hexadecane (3.54%), and 3-Hexanone, 2,2-dimethyl- (3.39%). These chemicals are useful in a number of industrial applications. For example, 4-tert-Butylcyclohexyl acetate is used in the preparation of high-loading fragrance encapsulation. Docosane is used in organic synthesis, calibration, and temperature sensing equipment. Earlier researchers reported that the degradation of hemicellulose and cellulose guides the formation of carboxylic and carbonyl compounds during the course of the pyrolysis process; however, phenols, cresols, and different aromatic compounds resulted due to the degradation of lignin [156]. Alkanes were responsible because of the extractive content of the biomass, whereas N_2-containing compounds cause the formation of NO_x during the combustion. The bio-oil can be used for domestic cooking purposes or as a source to extract valuable chemicals. However, it requires further treatment to improve its fuel quality and reduce corrosiveness before it can be used as an alternative to diesel.

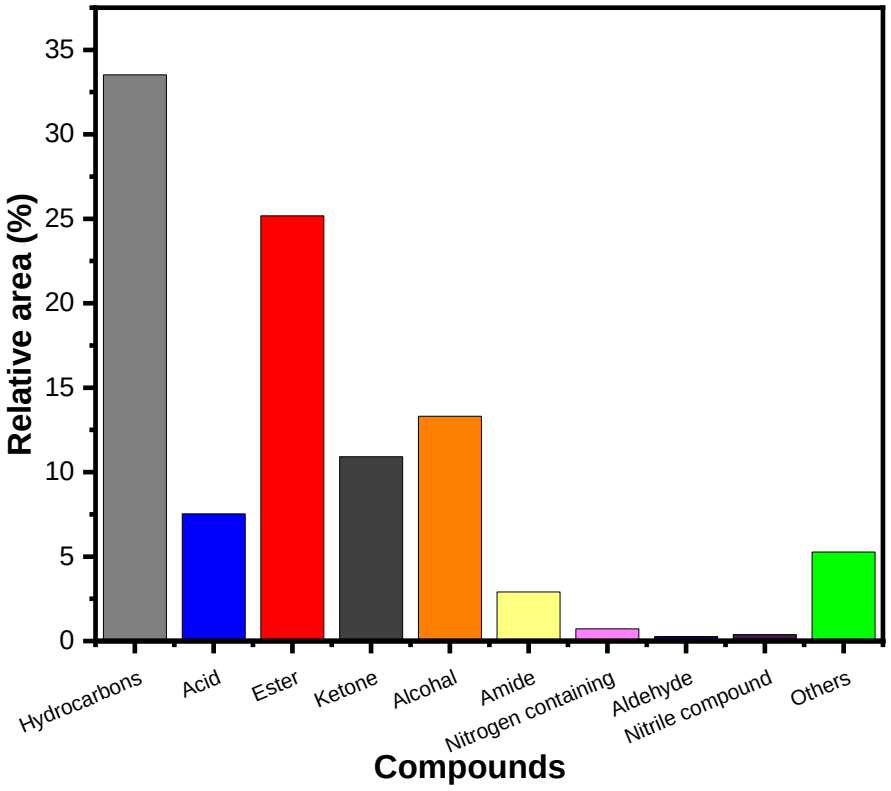

Fig. 5.7: GCMS analysis of MS bio-oil

5.9 Conclusion

The thermal degradation behavior and optimization of pyrolysis process variables of MS biomass were investigated. The kinetic result suggested that pyrolysis followed a complex reaction mechanism, and with an upsurge in heating rate, TG thermograph shifted towards the upper-temperature province without affecting the degradation pattern. The ANOVA technique confirmed that temperature affected the bio-oil yield more than the gas flow and heating rates. The highest bio-oil yield of 44.69% was found at optimum operating conditions. The results showed that the MS biomass could be a very good feedstock for recovering energy and value-added products through the thermal conversion route.